AFRL-SR-AR-TR-05-

0031

REPORT DOCUMENTATION PAGE

1. REPORT DATE (DD-MM-YYYY)	2. REPORT TYPE	3. DATES COVERED (From - To)
10-11-2004	Final	15/08/2001 - 14/08/2004

4. TITLE AND SUBTITLE
Computational Analysis and Simulation of Toxic Particle Deposition in the Human Respiratory System

5a. CONTRACT NUMBER
F49620-01-1-0492

5b. GRANT NUMBER

5c. PROGRAM ELEMENT NUMBER

6. AUTHOR(S)
Kleinstreuer, Clement
<ck@eos.ncsu.edu>

5d. PROJECT NUMBER

5e. TASK NUMBER

5f. WORK UNIT NUMBER

7. PERFORMING ORGANIZATION NAME(S) AND ADDRESS(ES)
North Carolina State University
Raleigh, NC 27695-7910

8. PERFORMING ORGANIZATION REPORT NUMBER

9. SPONSORING / MONITORING AGENCY NAME(S) AND ADDRESS(ES)
Dr. Walter J. Kozumbo
AFOSR Chemistry & Life Sciences
4015 Wilson Blvd., Rm712
Arlington, VA 22203-1954

10. SPONSOR/MONITOR'S ACRONYM(S)

11. SPONSOR/MONITOR'S REPORT NUMBER(S)

12. DISTRIBUTION / AVAILABILITY STATEMENT
The U.S. Government is authorized to reproduce and distribute reprints for Governmental purposes notwithstanding any copyright notation thereon.
Approve for Public Release: Distribution Unlimited

13. SUPPLEMENTARY NOTES

14. ABSTRACT

Jet fuel with its performance enhancers is highly toxic and when inhaled may pose a significant health risk. Thus, for a scientific assessment of possible health effects from fuel exposure, it is crucial to know where and at what concentrations fuel aerosols and their vapors deposit in the human respiratory system in light of realistic inlet conditions. In contrast to human testing, and/or experimental deposition studies, computational fluid-particle dynamics (CFPD) simulations offer a non-invasive, less expensive, and effective means of obtaining fuel vapor and droplet transport and deposition data for representative airways.

Focusing on JP-8 fuel deposition in a representative human upper airway model, experimentally validated CFPD results are provided for the airflow fields, JP-8 fuel droplets, and JP-8 fuel vapor under realistic ambient conditions. The 3-year-project conclusions, documented in 14 journal articles and 10 conference papers, are divided into three sections, i.e., fundamentals/discoveries, JP-8 fuel impact, and technology transfer.

15. SUBJECT TERMS
JP-8 fuel droplets, vapor; human lung deposition; computational fluid-particle dynamics; aerosol deposition efficiencies; vapor surface concentration

16. SECURITY CLASSIFICATION OF:			17. LIMITATION OF ABSTRACT	18. NUMBER OF PAGES	19a. NAME OF RESPONSIBLE PERSON
a. REPORT	b. ABSTRACT	c. THIS PAGE			Clement Kleinstreuer
U	U	U	UU	27	19b. TELEPHONE NUMBER (include area code) 919-515-5261

Standard Form 298 (Rev. 8-98)
Prescribed by ANSI Std. Z39.18

20050218 073

Table of Contents

Computational Analyses and Simulation of Toxic Particle Deposition in the Human Respiratory System

1. INTRODUCTION

As recently reviewed (see COT/NA, 2003), jet fuel performance enhancers, i.e., additives such as BHT, DiEGME, EGME, BTEX, etc., are highly toxic and may pose a significant health risk to Air Force personnel, fuelers, and people living near military fields. In order to understand the possible health effects from fuel exposure in form of inhaled droplets and vapor, it is crucial to know where and at what concentrations fuel aerosols and their vapors deposit in the human respiratory system, given a set of realistic inlet conditions.

Direct deposition tests of toxic fuel in human lung airways are impossible, and usually cost-intensive experimental deposition data lack any *detailed* resolution. Thus, computational fluid-particle dynamics (CFPD) simulations offer a non-invasive, less expensive, and effective means of obtaining fuel vapor and droplet transport and deposition data for representative airways. The human respiratory system has very complicated structures. The oral and nasal airways are two aerosol entries into the trachea. After the trachea, the tracheobronchial airways may be approximated as a network of repeatedly bifurcating tubes with progressively decreasing dimensions (Weibel, 1963). So far, computational airflow and particle transport simulations have concentrated on selected parts of the respiratory system. CFPD studies of micro-size particle deposition in human oral airways and tracheobronchial airways, employing single, double and triple bifurcating models have been extensively conducted by several research groups (Balásházy et al., 1999; Comer et al., 2001a, b; Kleinstreuer and Zhang, 2003; Zhang et al., 2002a, b; among others). These studies assumed that the size of inhaled particles stays constant in the respiratory tract. However, in many situations, solid or liquid particles undergo size changes because they absorb moisture or lose mass due to hygroscopity or evaporation. The effect of hygroscopity on deposition fraction in the human respiratory system has been investigated experimentally and theoretically (Broday and Georgopoulos, 2001; Ferron et al., 1988; 1989; Finlay and Stapleton, 1995; Gebhart et al., 1990; Hickey and Martonen, 1991; Morrow, 1986; among others). For example, hygroscopity can substantially increase the size and hence the airway deposition fraction of drug particles with initial dry sizes of about 0.5-2μm (Ferron et al., 1989). In contrast, as highly volatized compounds, jet fuel droplets vaporize quickly and may undergo dramatic size reduction as they move through the respiratory tract.

Focusing in this report on JP-8 fuel droplet and vapor deposition in a human upper airway model, the contrasting deposition pattern between aerosols and vapor as well as the resultant exposure risk are of interest. Considering different inspiratory flow rates, droplet trajectories,

evaporation and deposition are modeled with Newton's Second Law and scalar equations, i.e., using a decoupled Euler-Lagrange approach, whereas fuel vapor transport and deposition is described with a modified mass transfer equation, i.e., in an Eulerian framework (see Kleinstreuer, 2003).

2. THEORY

2.1 Airway Geometry

The detailed descriptions about the present upper airway model are given in Zhang & Kleinstreuer (2003b), which includes oral cavity, pharynx, larynx and trachea, and a symmetric triple bifurcation lung airway representing generations G0 (trachea) to G3 after Weibel (1963).

2.2 Governing Equations

2.2.1 Airflow and heat transfer

In order to capture the air flow structures in the laminar-to-turbulent flow regimes, i.e., $300<Re_{local}<10^4$ for the present airway configuration and a wide range of inhalation flow rates ($15\leq Q_{in} \leq 60$ l/min), the low-Reynolds-number (LRN) k-ω model of Wilcox (1993) was selected and adapted which has been demonstrated to be appropriate for such internal flows (Zhang & Kleinstreuer, 2003a). As demonstrated by Zhang et al. (2002a, b), the transient fluid-particle dynamics can be accurately matched assuming steady flow, i.e., using equivalent Reynolds-and-Stokes-number pairs for all inhalation flow rates. All air flow equations, as well as initial and boundary conditions, are given in Zhang & Kleinstreuer (2003a, b).

2.2.2 Transport of micro-size droplets

With any given ambient concentration of non-interacting spherical droplets, a Lagrangian frame of reference for the trajectory computations of the evaporating droplets can be employed. The detailed descriptions of micro-particle trajectory equation with turbulent dispersion are given in Zhang et al. (2005).

2.2.3 Droplet evaporation

This analysis considers that the droplet temperature and composition are maintained spatially uniform but evolve with time and the droplet remains spherical during vaporization. This assumption is reasonable because of the small Biot number ($Bi<<1$) for the micro-size droplets. Considering the convective heat and mass transfer over the whole surface of the spherical droplets, the change in droplet mass (or size) can then be calculated (see Zhang et al., 2004).

2.2.4 Mass transfer of vapor or ultrafine particles.

The convection mass transfer equation of ultrafine particles, or (JP-8) fuel vapor, whose dominant radial transfer mechanisms are Brownian motion and turbulent dispersion can be given as (Zhang & Kleinstreuer, 2003b, 2004):

$$\frac{\partial Y}{\partial t}+\frac{\partial}{\partial x_j}\left(u_j Y\right)=\frac{\partial}{\partial x_j}\left[\left(\widetilde{D}+\frac{\nu_T}{\sigma_Y}\right)\frac{\partial Y}{\partial x_j}\right] \tag{1}$$

where Y is the mass fraction, $\sigma_Y = 0.9$ is the turbulence Prandtl number for Y. JP-8 fuel is a multi-component mixture which consists mainly of C8 to C16 paraffinic hydrocarbons with other hydrocarbons and additives also present; however, the diffusivity in air does not vary significantly from compound to compound (Gustafson et al., 1997). Thus, the conservative assumption presently implemented was to set $\widetilde{D} = 0.05$ cm^2/sec for all fractions of JP-8 jet fuel at T=293K with little loss in accuracy according to Gustafson et al. (1997). The effect of temperature change on diffusivity is expressed by the following semi-empirical correlation (Bejan, 1995):

$$\widetilde{D}(T)/\widetilde{D}(T=293K)=(T/293)^{1.75} \tag{2}$$

The aerosol diffusion coefficient is calculated as follows (Finlay, 2001):

$$\widetilde{D}_p=(k_B T C_{slip})/(3\pi\mu d_p) \tag{3}$$

where k_B is the Boltzmann constant (1.38×10^{-23} J K^{-1}); and C_{slip} is the Cunningham slip correction factor.

Assuming that the airway wall is a perfect sink for aerosols or vapors upon touch, the boundary condition on the wall is Y_w=0. This assumption is reasonable for fast gas-wall reaction kinetics (Fan et al., 1996), or vapors of high solubility and reactivity, and also suitable for estimating the maximum deposition of toxic vapor in the airways. For less soluble vapors, the wall concentration would be greater than zero so that transport in tissue and in airways must be considered simultaneously for simulating vapor uptake. Assuming that the surface of respiratory epithelium is covered by a mucus layer with uniform thickness and a lipid layer lie below the mucus lining simulating the transport barrier by the epithelial cell membrane, Keyhani et al. (1997) derived a flux condition at the airway boundary including the vapor transport in the tissue. This boundary condition was inferred from the mass conservation and mass diffusion of vapor from the airway to the mucus layer and to the tissue, which is given as:

$$D_{in}\frac{\partial Y}{\partial n}+KY=0 \tag{4}$$

where D_{in} is the inlet tube diameter, n is the direction normal to the airway wall, and K is a dimensionless parameter, here we call it absorption parameter, which is defined as

$$K = \frac{D_{in}\tilde{D}_m\xi}{\tilde{D}_a\beta\tanh(\xi H_m)}\left[1-\frac{2\tilde{D}_m/H_m}{(\tilde{D}_m/H_m+P_l)(e^{\xi H_m}-e^{-\xi H_m})}\right] \quad (5)$$

where $\tilde{D}_a, \tilde{D}_m$ are the vapor diffusivity in the air and the liquid mucus phase, respectively; H_m is the thickness of the mucus layer; and β is the equilibrium partition coefficient for a given contaminant molecular, which can be determined by Henry"s law; $\xi = \sqrt{k_r/\tilde{D}_m}$ with k_r being a single rate constant considering the chemical reactions of vapors in the mucus layer; $P_l = \gamma\tilde{D}_l/H_l$ is the lipid permeability coefficient with $\gamma, \tilde{D}_l, H_l$ being lipid-mucus partition coefficient, vapor diffusivity in the lipid and the thickness of the lipid layer, respectively.

Clearly, for a highly soluble ($\beta \to 0$) or high reactive ($k_r \to \infty$) vapor, the boundary condition (4) reduces to Y=0. If vapor is insoluble ($\beta \to \infty$), the boundary condition reduces to the zero mass flux condition, i.e., $\partial Y/\partial n = 0$. Ignoring removal of contaminant molecules in the mucus by chemical reaction and the resistance to transport across the lipid barrier, the absorption parameter K reduces to:

$$K = \frac{D_{in}\tilde{D}_m}{\tilde{D}_a\beta H_m} \quad (6)$$

2.3 Deposition Parameters

The regional deposition of micro-droplets in human airways can be quantified in terms of the deposition fraction (DF) or deposition efficiency (DE) in a specific region (e.g. oral airway, first, second and third bifurcations etc.); they are defined as:

$$DF_{particle} = \frac{Number\ of\ deposited\ particles\ in\ a\ specific\ region}{Number\ of\ particles\ entering\ the\ mouth} \quad (7)$$

$$DE_{particle} = \frac{Number\ of\ deposited\ particles\ in\ a\ specifc\ region}{Number\ of\ particles\ entering\ this\ region} \quad (8)$$

The DEs and DFs are the same for the oral airway model in this study.

The deposition fraction (DF) of vapors or ultrafine particles can be calculated with the regional mass balance or the sum of local wall mass flux. According to the mass balance in one specific region, DF is defined as:

$$DF = 1-(\sum_{i=1}^{n}\int u_i Y_i dA_i)/(\int u_0 Y_0 dA_0) \quad (9)$$

where A is the tube cross sectional area, and u is the axial velocity. The subscripts "0" and "i" denote the properties at the inlet and the *ith* daughter tube of a selected generation, respectively. In the oral airway model, the "*i*" denotes the trachea and *n=1*.

As for the local wall mass flux of vapors, it can be determined as

$$\dot{m}_w = -\rho A_i (\tilde{D} + \frac{\nu_T}{\sigma_Y}) \frac{\partial Y}{\partial n}\Big|_i \tag{10}$$

where A_i is the area of local wall cell (i). The local vapor deposition fraction, which is defined as the ratio of local wall mass flux to the inlet mass flux, can be expressed as

$$DF_{local} = [-A_i (\tilde{D} + \frac{\nu_T}{\sigma_Y}) \frac{\partial Y}{\partial n}\Big|_i] / (Q_{in} Y_{in}) \tag{11}$$

and the regional deposition fraction can be determined as

$$DF_{region} = \sum_{i=1}^{n} [-A_i (\tilde{D} + \frac{\nu_T}{\sigma_Y}) \frac{\partial Y}{\partial n}\Big|_i] / (Q_{in} Y_{in}) \tag{12}$$

where n is the number of wall cells in one specific airway region, e.g., oral airway, first airway bifurcation, etc. The local vapor deposition patterns can be quantified in terms of a deposition enhancement factor (DEF) (cf. Balashazy et al., 1999, 2003), which is defined as the ratio of local to average deposition densities, i.e.,

$$DEF = [(\tilde{D} + \frac{\nu_T}{\sigma_Y}) \frac{\partial Y}{\partial n}\Big|_i] / \{\sum_{i=1}^{n} [A_i (\tilde{D} + \frac{\nu_T}{\sigma_Y}) \frac{\partial Y}{\partial n}\Big|_i] / \sum_{i=1}^{n} A_i\} \tag{13}$$

DEF indicates vapor deposition "hot spots" in a given region.

2.4 Numerical Method

The numerical solutions of the governing equations including flow, heat and mass transfer equations were carried out with a user-enhanced finite-volume based program, i.e., CFX4.4 from ANSYS, Inc., previously AEA Technology (2001). The numerical program uses a structured, multiblock, body-fitted coordinate discretization scheme (Zhang & Kleinstreuer, 2002). A Higher-Order Upwind (HUW) differencing scheme, which is second-order accurate in space, was used to model the advective terms of the transport equations. The sets of linearized and discretized equations for all variables were solved using the Block Stone's method.

The droplet transport and evaporation equations were also solved with the commercial software in combination with user-supplied programs. The particle trajectory equations were solved using Gear's BDF method. After each iteration for each particle, the information about position, time, diameter, temperature and three components of the velocity as well as the speed with which the particles cross the control volume boundaries was obtained. Droplet deposition occurs when its center comes within a radius from the wall, i.e., local surface effects such as

droplet evaporation (blowing), migration, or resuspension have been currently ignored. In the present model the number of particles, n≅10,000, was determined by increasing the inlet particle concentration until the deposition fraction became independent of the number of particles simulated.

The computational mesh was generated with CFX Build4. The near-wall region required a very dense mesh. Specifically, the thickness of the near-wall cells was chosen to fully contain the viscous sub-layers and to resolve any geometric features present there. The mesh topology was determined by refining the mesh until grid independence of the flow field solution and particle deposition fractions was achieved. The final mesh contains about 420,000 and 670,000 cells for the oral airway and four-generation airway model, respectively. The computations were performed on an SGI Origin 2400 workstation with 32GB RAM and multiple 450 MHz CPUs. The steady-state solution of the flow field was assumed to be converged when the dimensionless mass residual, (Total Mass Residual)/(Mass Flow Rate) $< 10^{-3}$. The convergence of k and ω was monitored as well. Typical run time for the fluid flow, energy and mass transfer simulations on eight processors with parallel algorithm was approximately 24 hours for the oral airway model and 8 hours for the four-generation model. Utilizing the converged flow field solution, the droplet trajectory simulations required approximately 4 to 6 hours for each case considered.

3. RESULTS

3.1 Model Validations

For accurate computational fluid-particle dynamics (CFPD) simulations, matching comparisons with theoretical or experimental fluid velocity profiles, pressure drops and local particle distributions are necessary. Our CFPD model has been validated with various experimental data sets for steady and transient laminar flows in bifurcations (Comer et al, 2001a; Zhang & Kleinstreuer, 2002) and for laminar, transitional and turbulent flows in tubes with local obstructions (Kleinstreuer & Zhang, 2003; Zhang & Kleinstreuer, 2003a). Especially, the low-Reynolds-number (LRN) k-omega model has been extensively validated and has been proven to be an applicable approach to capture the velocity profiles and turbulence kinetic energy for laminar-transitional-turbulent flows in the constricted tubes of the upper airways (see Zhang & Kleinstreuer, 2003a). Similarly, the simulated spherical, micro-particle depositions in airways were successfully compared with measured deposition efficiencies and deposition patterns (Comer et al., 2001b; Zhang et al., 2002a-d). The simulation of spherical, nanoparticle deposition due to diffusional transport has been validated with both analytical solutions in straight pipes and experimental data for a double-bifurcation airway model (Shi et al., 2004) as well as experimental data in an oral airway model (Zhang & Kleinstreuer, 2003b). For example, particle

deposition fractions as a function of Stokes number are compared with the observations by Cheng et al. (1999) in Fig. 1 for three inhalation rates. The Stokes number is defined here as by Cheng et al. (1999), i.e., $St=\rho_p d_p^2 U/9\mu D$, with ρ_p being the particle density, d_p being the particle diameter, and U being the mean velocity evaluated as (Q/A), where A is the mean cross-sectional area, and D is the minimum hydraulic diameter. The validation result for droplet vaporization simulations is given in Fig. 2. The simulated temporal diameter variation of a JP-8 fuel droplet is compared with experiment measurements conducted by Runge et al. (1998), where a JP-8 fuel droplet with an initial diameter of 639μm was suspended in 294K air moving at a constant speed of 3m/s. It can be seen that the simulated vaporization law for JP-8 fuel, using $D_{effective}=0.05 cm^2/sec$, is in excellent agreement with experimental data.

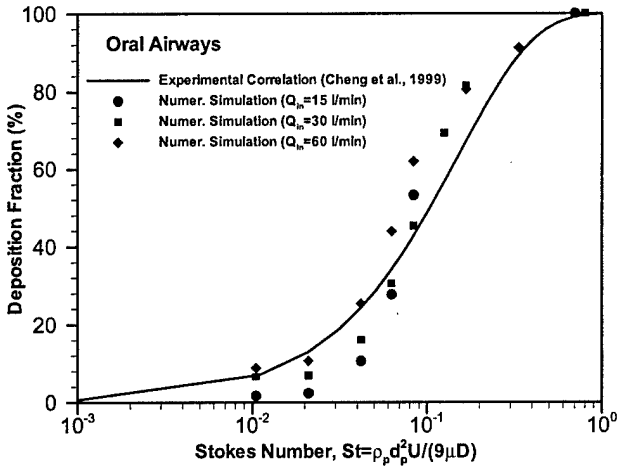

Fig. 1: Comparison of simulated fine particle deposition fractions in the oral airway model with the experimental data of Cheng et al. (1999).

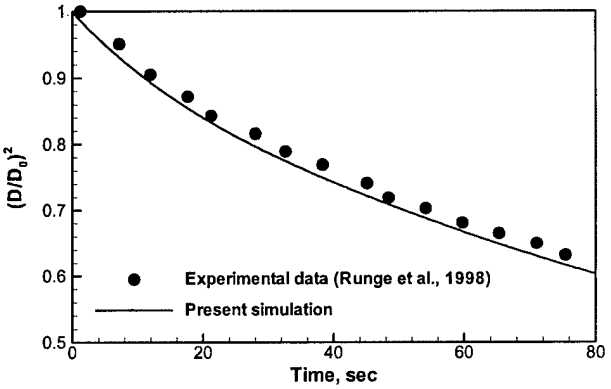

Fig. 2: Comparison of diameter evolution for a JP-8 droplet with the experimental data of Runge et al (1998).

In summary, the good agreements between experimental findings and theoretical predictions instill confidence that the present computer simulation model is sufficiently accurate to analyze transport and deposition of toxic particle/droplet and vapor in three-dimensional oral and upper bronchial airways associated with laminar-to-turbulent airflows.

3.2 Airflow Fields

Some selected results from our simulations for different inspiratory flow rates and inlet air temperatures are given below. Figures 3a and 3b show mean velocity profiles in an oral airway model starting from mouth to trachea and a bifurcating airway model G0 to G3 (G0 is the trachea) with an inspiratory flow rate of Q_{in}=30 l/min and T_{in}=310K, respectively. The selected cross-sectional views display the axial velocity contours as well as secondary velocity vectors. Clearly, skewed velocity profiles generated by the centrifugal force can be observed in the curved portion from the oral cavity to the pharynx/larynx. Moreover, a central asymmetric jet and a recirculation zone are created in the laryngeal region because of the restriction of the (assumed stationary) vocal folds. The secondary motion is set up when the flow turns a bend from the mouth to the pharynx because of the centrifugally induced pressure gradient (see Kleinstreuer & Zhang, 2003). Turbulence may locally occur during this medium-level breathing (Q_{in}=30 l/min), where the turbulent fluctuations are weak in the oral cavity; but, they becomes strong after the constriction of soft palate and rises rapidly after the glottis, eventually decaying more slowly while approaching an asymptotic level. With further redistribution of the kinetic energy of the flow over most of the cross section accompanied by the onset of turbulence, the velocity profiles become more blunt from the left to the right wall, and the maximum velocity zone moves to the anterior wall at the cross section six diameters from the glottis (see Fig. 3a). Fig. 3b shows the mean-velocity fields in the planar triple-bifurcation airways which are physiologically 90° turned with respect to the oral airways. The velocity profiles and turbulence quantities extracted from the trachea in the oral airway model were adjusted as the inlet conditions for the bifurcating airway model G0 to G3. The air stream in the branching airways splits at each flow divider and new boundary layers are generated at the inner walls of the daughter tubes. The velocity profiles are naturally skewed in each daughter tube, and hence, each daughter tube, or generation, may experience a different flow rate. The primary characteristics of the flow fields at cross sections C-C′, D-D′, and E-E′ are quite similar; specifically: (i) skewed velocity profiles with the maximum velocity near the inner wall around the divider; and (ii) two distinct secondary vortices appearing at the upper and lower side of the tube, which moves the high speed fluid up around the top of the tube towards the outside of the bifurcation and low speed fluid from the outside of the bifurcation along the symmetry plane towards the inside of the bifurcation.

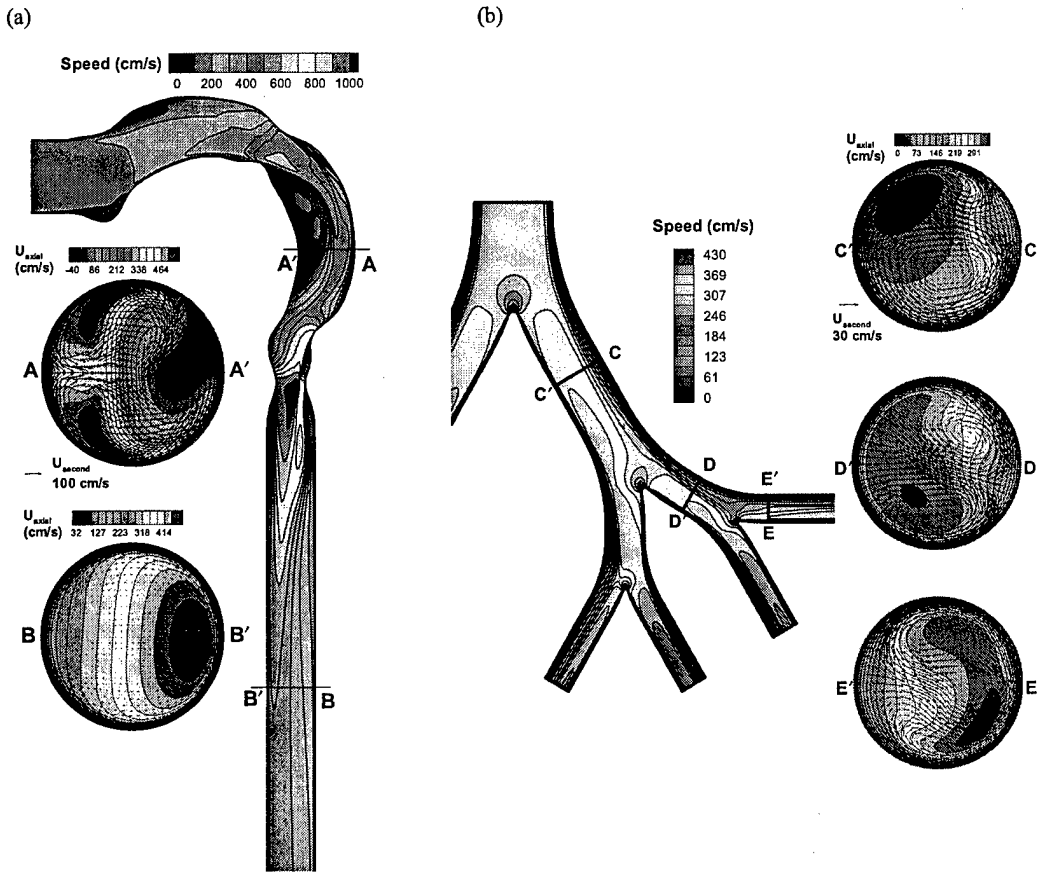

Fig.3: Side-plane or mid-plane velocity profiles as well as selected cross-sectional axial velocity contours and secondary velocity vectors with an inspiratory flow rate Q_{in}=30 l/min in: (a) an oral airway model; and (b) a bifurcating airway model G0 to G3.

The details about the airflow structures and particle distributions in both oral and tracheobronchial airways under cyclic breathing conditions as well as the effects of airway geometric features, inspiratory flow rate and thermal condition of incoming air can be found in Zhang & Kleinstreuer (2002, 2003b), Zhang et al. (2002d, 2004).

3.3 JP-8 Fuel Aerosols

Inertial impaction is the main deposition mechanism for micron-size droplets; hence, particle size greatly affects droplet deposition. However, jet fuel is a multi-component liquid and the C8 to C11 fractions are especially volatile. Here, one extreme case is presented, i.e., it is assumed that the inlet vapor fraction of JP-8 fuel is zero and the background concentration of

vapor, created by droplet evaporation, is negligible. Clearly, the diameter of each droplet decreases gradually in the airways due to the loss of its mass by evaporation which is a function of the airflow momentum as well as the droplet heat and mass transfer. Affected by the highly non-uniform, occasionally turbulent airflow structures in the oral airways, the trajectories for different droplets vary; hence, the changes of droplet diameters are different because of the different local airflow as well as heat and mass transport. Thus, droplets enter the mouth monodisperse but turn polydisperse during vaporization. Figure 4 shows the cumulative distribution function of the droplet size at the outlet of the oral airways, or the inlet to the first bifurcation, for different inhalation rates and inlet air temperatures. The fraction less than a particular size can be obtained directly from the graph. The fraction of particles having diameters between two sizes can be determined by the difference of the cumulative fractions at these two sizes. The initial droplet size is a uniform distribution with $d_p = 5\mu m$. As expected, the change of droplet size decreases with increasing flow rate due to decreasing residence times. The variation of the droplet size is larger with higher inlet air temperature because the saturation vapor pressure at the liquid/gas interface increases with temperature. The mean droplet diameters after the oral airways are d_p=4.03, 4.57, 4.83 μm for Q_{in}=15, 30, 60 l/min with T_{in}=263K, respectively, and d_p=2.80 μm for Q_{in}= 30 l/min with T_{in}=310K. The variations in droplet size should greatly influence droplet deposition.

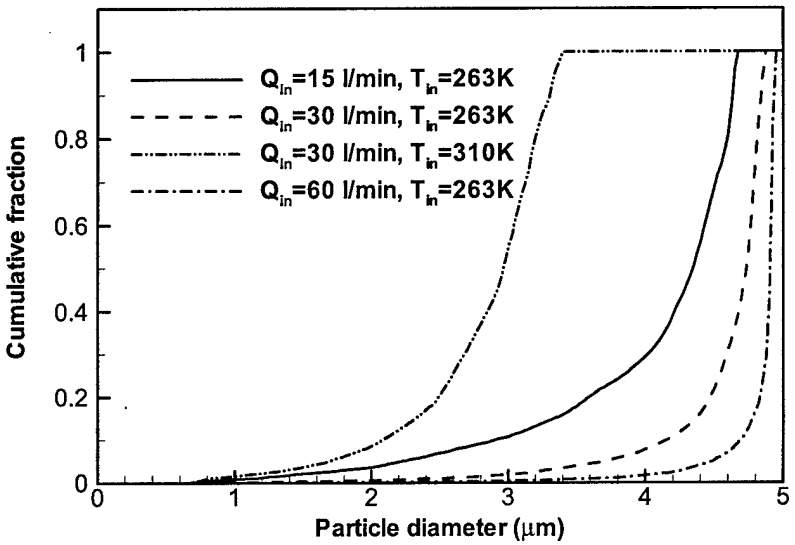

Fig. 4: Cumulative distribution of JP-8 fuel droplet sizes at the inlet of the bifurcation airway model.

The local deposition patterns in the oral airway model are shown in Fig. 5 for initially d_p=5μm and Q_{in}=30 l/min with and without evaporation. Due to inertial impaction, droplets mainly deposit at stagnation points for axial particle motion, such as the tongue portion in the oral cavity, the outer bend of the pharynx/larynx, and the regions just upstream of the glottis. A few droplets may also deposit outside these pronounced regions, being influenced by turbulent dispersion as well as secondary and recirculating flows. Clearly, droplet deposition decreases due to the reduced droplet diameters with evaporation.

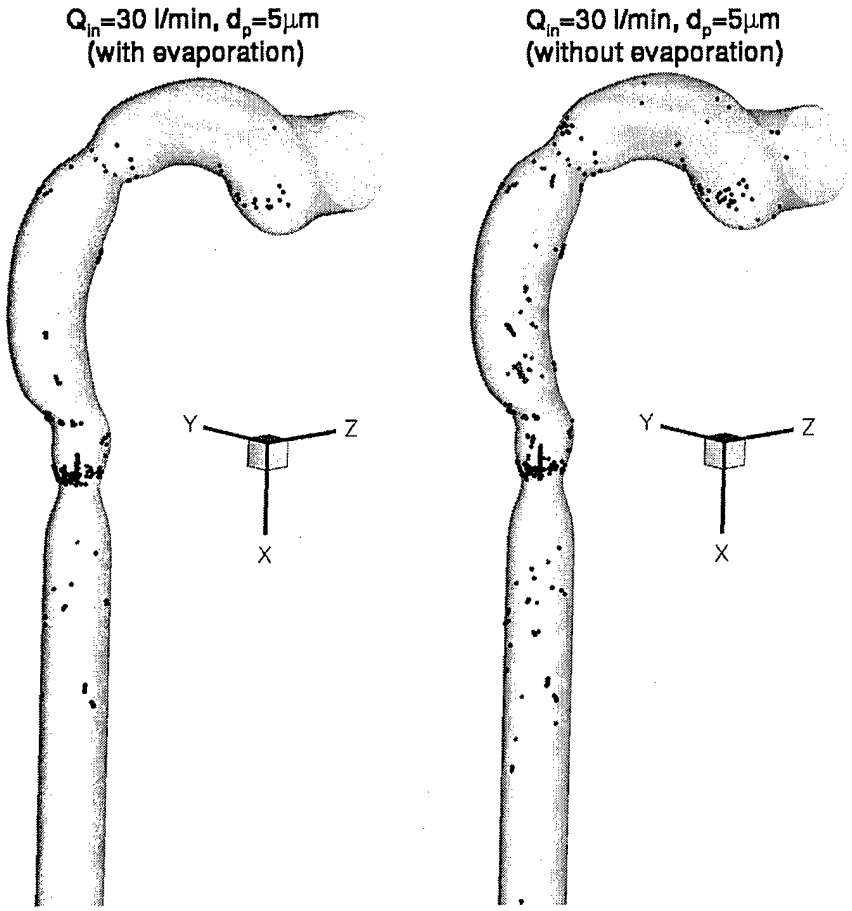

Fig. 5: Droplet deposition patterns in the oral airway model.

Droplet evaporation is very important in simulating the deposition of volatile aerosols, e.g., JP-8 fuel droplets, in human airways. This also can be seen from the comparisons of predicted droplet deposition fractions (DF) in the oral airways for different inhalation conditions (see Fig. 6). Figure 6 indicates that the DFs of droplets decrease significantly if vaporization

occurs. The DF increases with increasing initial particle diameter and inhalation flow rate due to enhanced inertial impaction (Fig. 6).

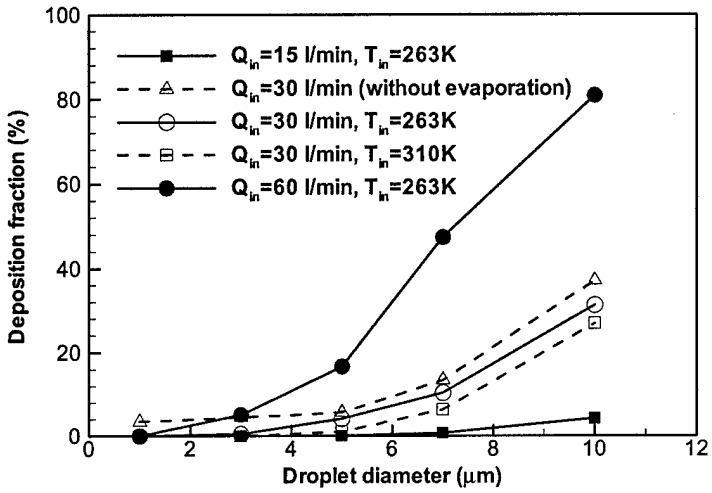

Fig. 6: Deposition fractions of JP-8 fuel droplets in the oral airway model.

Figure 7 depicts the overall droplet deposition efficiency (DE) in the upper bronchial airways (G0-G3), which is defined as the number of deposited droplets to that entering at the inlet of airway segment G0 to G3. The deposition efficiency with evaporation (T_{in}=263K) is still lower than that without evaporation. There is no droplet deposition for the case of d_p= 3 μm with evaporation. The percent decrease in the deposition efficiency due to evaporation is higher for the relatively smaller size droplets (say, 3 and 5μm). This is because large size particles tend to shrink much slower than smaller particles. The overall DE in G0 to G3 with an ideal inlet condition, i.e., fully-developed air flow with corresponding (parabolic) particle distribution, is also given in Fig. 7 for comparison. Clearly, the inlet air velocity profile and particle distribution strongly affect the particle deposition efficiency, where idealized inlet flow conditions may overpredict actual deposition efficiencies. However, regardless of the simulated cases, micro-size particles tend to deposit at the carinal ridges in the bronchial airways due to inertia impaction (see Fig. 8 for droplets in the present case, and Fig. 4 in Zhang et al. (2002b) for solid particles).

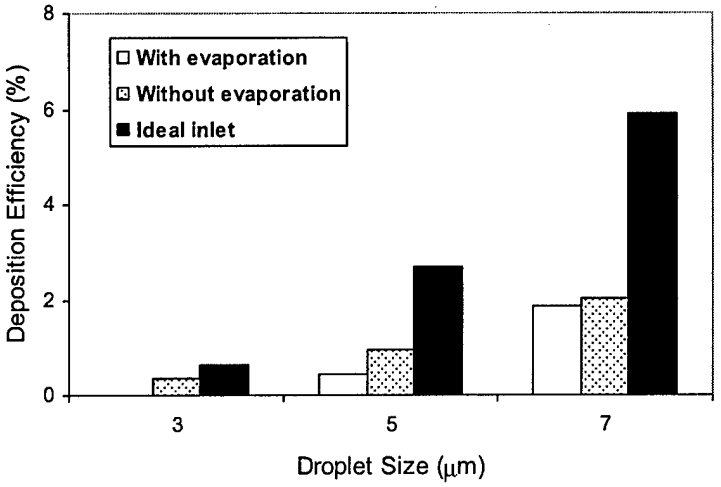

Fig. 7: Deposition efficiencies of JP-8 fuel droplets in the bifurcation airway model with an inspiratory flow rate Q_{in}=30 l/min. The inlet air temperature is 263K for the evaporation case.

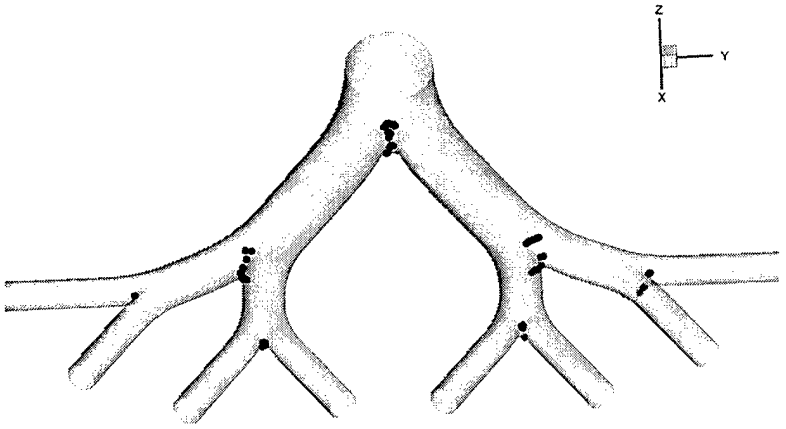

Fig. 8: Droplet deposition patterns in the bifurcation airway model (Q_{in}=30 l/min). Droplet diameter is 7μm at mouth inlet and evaporation is considered.

3.4 JP-8 Fuel Vapor

As aforementioned, the degree of vapor absorption by the airway wall may influence fuel vapor transport and deposition in the airways. Because JP-8 fuel is a multi-component mixture and the solubility of its components changes very largely (Gustafson et al., 1997), the absorption parameter K in Eq. (5) may vary from 10^{-3} to 10^{3} for different compounds. As a case for estimating the maximum deposition of toxic vapor in the airways, the following results are based on the perfect absorption assumption of vapor in the airway surface (i.e., Y_{wall}=0), except in

Section 3.4.4 which discusses the impacts of the absorption parameter K.

3.4.1 Distributions of mass fractions and deposition patterns

Figures 9a and 9b display the concentration contours of JP-8 fuel vapors in the oral airway and airway segment G0 - G3. A uniform inlet JP-8 vapor concentration condition was

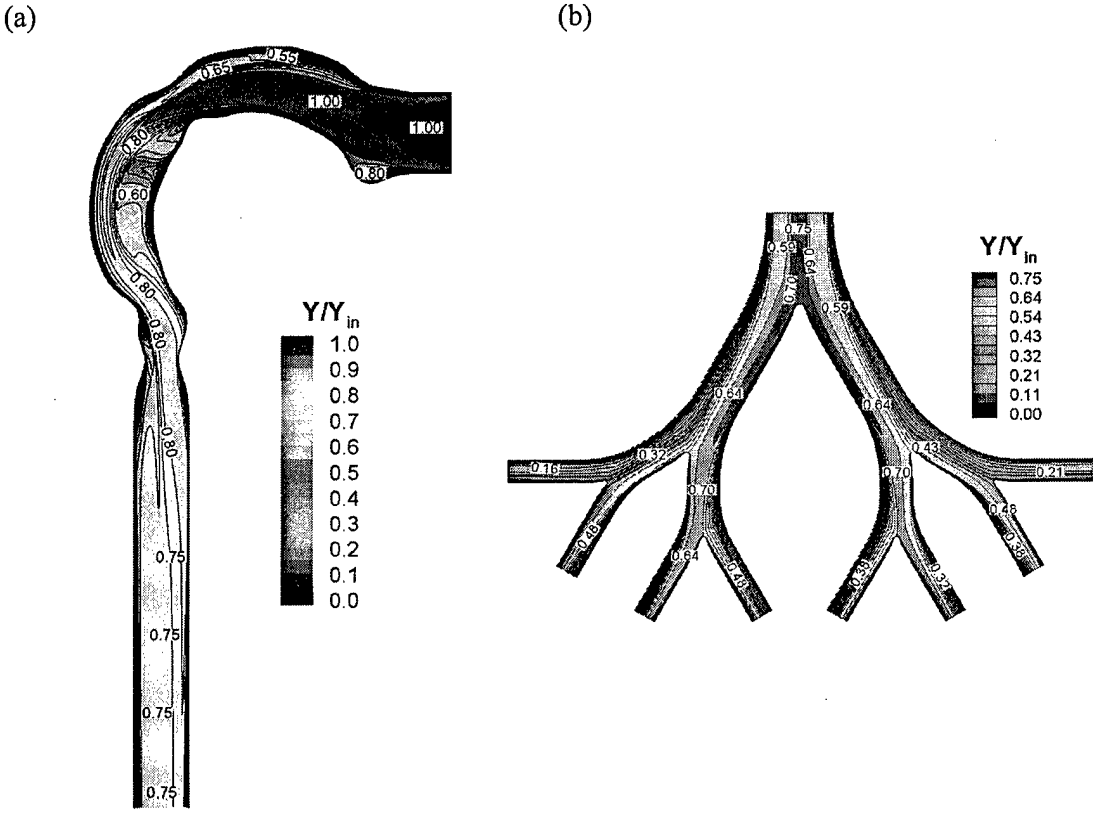

Fig. 9: Concentration contours of JP-8 vapor in at Q_{in}=15 l/min and T_{in}=263K in: (a) the oral airway model (y=0 plane); and (b) the bifurcation airway model (z=0 plane).

assumed. The distributions of vapor concentration are dependent of velocity profiles so that areas of low velocities are associated with low concentrations due to the low convective mass transfer. The local concentration gradient near the wall indicates the vapor deposition rate at that site. Thus, the local deposition rate tends to be high at the oral cavity and becomes low in the trachea due to the vapor redistribution over the cross sections driven by secondary and reverse flows. The vapor field in the trachea for Q_{in}=15 l/min cannot be mixed as rapidly as the heat, where the temperature distributions tend to be uniform at E-E′ and F-F′. This may be attributed to the relatively high Lewis number for JP-8 vapor (Le≅4). The thermal effect on concentration

distribution is apparent for this low inspiratory flow rate case, but it tends to be negligible for high flow rate cases (Q_{in}=30 and 60 l/min) (Zhang & Kleinstreuer, 2003b). In airway segment G0-G3, the mass transfer patterns are also strongly affected by the skewed, asymmetric velocity profiles which indicate different vapor deposition at different airway tubes.

Figure 10 shows examples of vapor deposition patterns in terms of distributions of DEF (see Eq. (13)) in the oral airway model and the bifurcation airway model. Clearly, the deposition patterns are somewhat inhomogeneous. In the oral airway model, the enhanced deposition may occur at the entrance, outside bend of the pharynx and the throat because of great degrees of mixing, i.e., large concentration gradients at these regions. Turning to the bifurcation airway model G0 to G3, the enhanced deposition mainly occurs at the cranial ridges and the inside walls around the carinal ridges due to the complicated air flows and large particle concentration gradients in these regions. Of interest is that the maximum DEF-values for vapor are much lower than those for micro-droplets, i.e., the DEF_{max} for micro-particles is of the order of 10^2 to 10^3 (see Zhang et al., 2005), while DEF_{max} for vapor is of the order of 1 (see Fig. 10). This indicates that the deposited vapor is much more uniformly distributed in the upper airways when compared to the micro-droplet deposition.

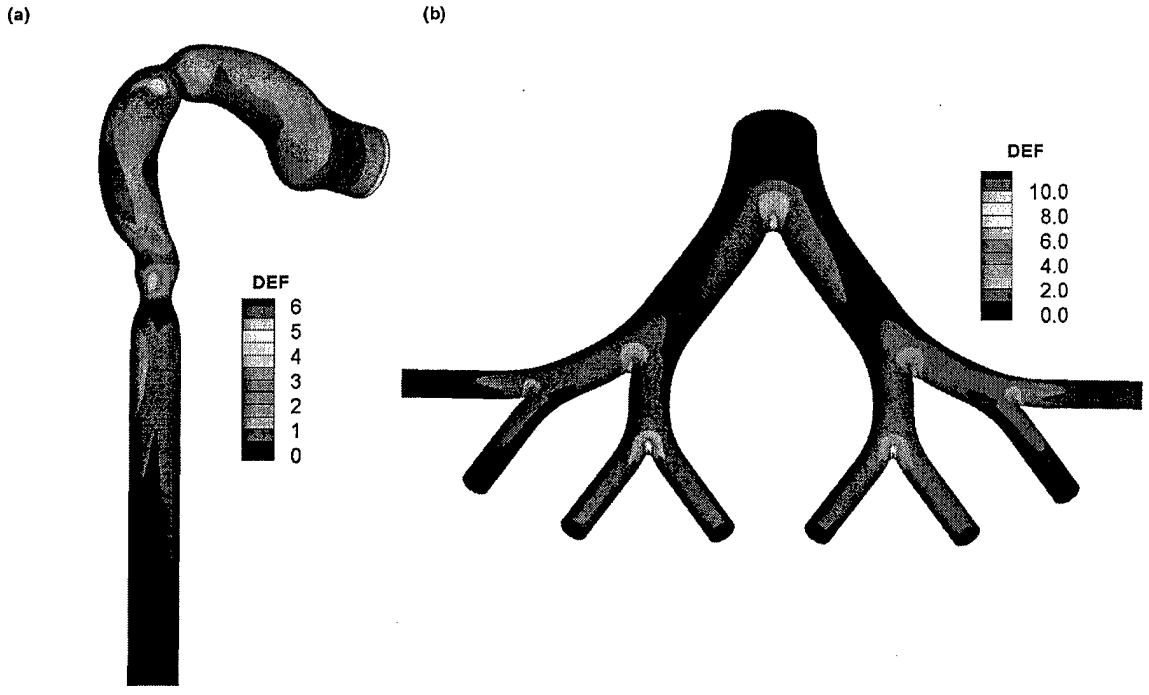

Fig. 10: 3-D distributions of deposition enhancement factor (DEF) of JP-8 fuel vapor under steady inhalation with Q_{in}=30 l/min in: (a) the oral airway model; and (b) the bifurcation airway model.

3.4.2 Deposition fractions of fuel vapor

The deposition fractions of JP-8 fuel vapor in the upper airways under different inhalation conditions are shown in Fig. 11a-c. It can be seen from Fig. 11a that higher vapor deposition corresponds to larger inlet air temperatures, especially for the high inhalation flow rate case. This can be attributed to the relatively large diffusion coefficient at relatively high temperatures (see Eq. (2)). Generally speaking, the deposition fraction is weakly affected by the inlet air temperature for both low and high inspiratory flow rates. In other words, the thermal effects could be negligible when calculating the total or segmental deposition fraction of vapors or ultrafine particles in the upper airways. The flow rate also shows a significant effect on the deposition of vapor (cf. Fig. 11b and c). The higher the flow rate, the lower is the deposition fraction. This may be because of the longer residence times for vapors with low flow rates and is consistent with the experimental observations of Li et al. (1998) for deposition of Iodine vapor in a tracheobronchial cast. The deposition fraction may increase 75% to 120% in the oral airways and G0 to G3 when switching from exercise breathing ($Q_{in} = 60$ l/min) to low-level breathing ($Q_{in} = 15$ l/min). The deposition fraction of JP-8 fuel vapor in the oral airway and G0 to G3 under resting condition can be as high as 36% and 25%, respectively.

3.4.3 Calculation of mass transfer coefficient

Calculation of the respiratory mass transfer coefficient, h_m, is helpful in quantitatively predicting the regional uptake of inhaled vapor (Cheng et al., 1997a, b). The mass balance for one airway unit is:

$$N \cdot A_{wall} = \sum_{i=1}^{n} \dot{m}_i Y_i - \dot{m}_0 Y_0 \tag{14}$$

which yields the wall mass flux of species N, so that

$$h_m = \frac{N}{\overline{\rho Y_m} - \rho Y_{wall}} \tag{15}$$

For simplicity, we only used the average values of the inlet and outlet cross-sectional mass fractions to determine the regional $\overline{\rho Y_m}$, i.e.,

$$\overline{\rho Y_m} = \frac{1}{2}\left[\frac{\int \rho_0 u_0 Y_0 dA_0}{\int \rho_0 u_0 dA_0} + \frac{1}{n}\sum_{i=1}^{n} \frac{\int \rho_i u_i Y_i dA_i}{\int \rho_i u_i dA_i} \right] \tag{16}$$

The Sherwood number (Sh), characteristic of convective dispersion, can be calculated as:

$$Sh = (h_m D)/\tilde{D} \tag{17}$$

The diameters in the trachea and the parent tubes are employed to determine the Sh-number for the oral airways and bifurcation units, respectively.

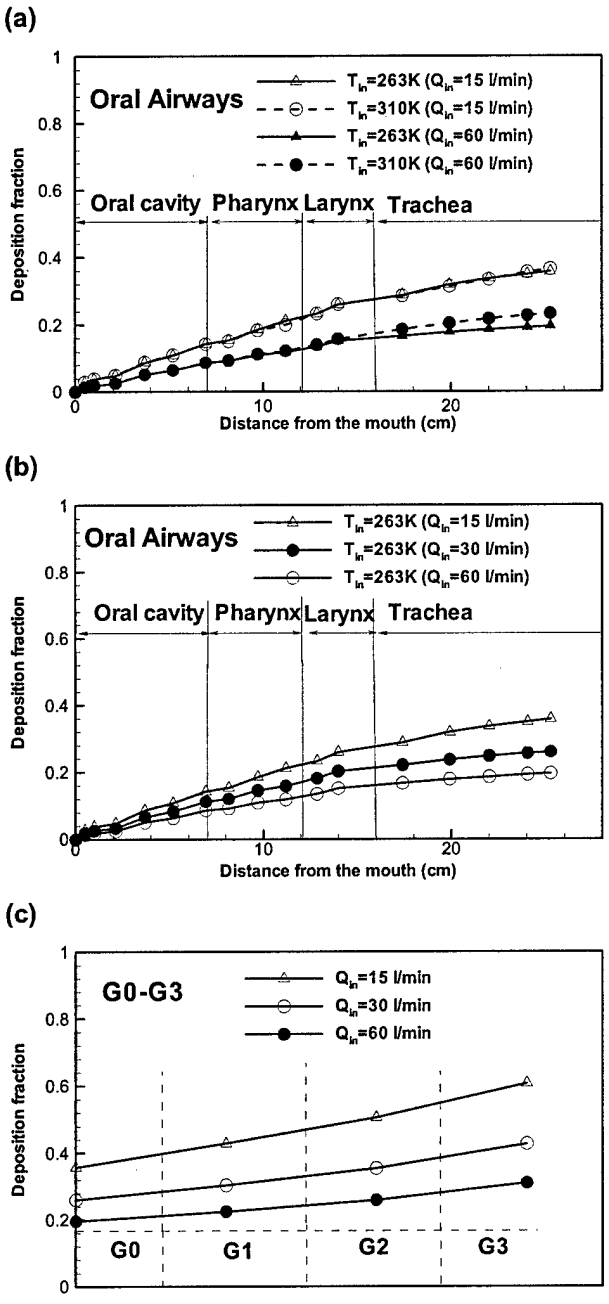

Fig. 11: Deposition fractions of JP-8 fuel vapor in the upper human airway

Figure 12a depicts the regional Sherwood number (Sh) for the oral airway model vs. the product of Reynolds (Re) and Schmidt (Sc) numbers, both evaluated in the trachea, based on different inhalation flow rates and diffusion coefficients (i.e., particle sizes). The correlation between Sh-number and ReSc-group can be expressed as:

$$Sh = 0.852(\mathrm{Re}\,Sc)^{0.405} \qquad 1500 < \mathrm{Re} < 7000,\ 1 < Sc < 230 \tag{18}$$

where r^2=0.99. The convective mass transfer coefficients for JP-8 fuel vapor in terms of the Sh-number has been also obtained for each individual bifurcation in airway generations G0 to G3 (Fig. 12b). Affected by the non-homogeneous airflow structures and mass concentration distributions, the regional Sh-numbers are slightly different for each bifurcation. However, a best-fit correlation yielded (Fig. 12b):

$$Sh = 1.727(\mathrm{Re}\,Sc)^{0.328} \qquad 600 < \mathrm{Re} < 6000,\ Sc \approx 3 \tag{19}$$

where r^2=0.77.

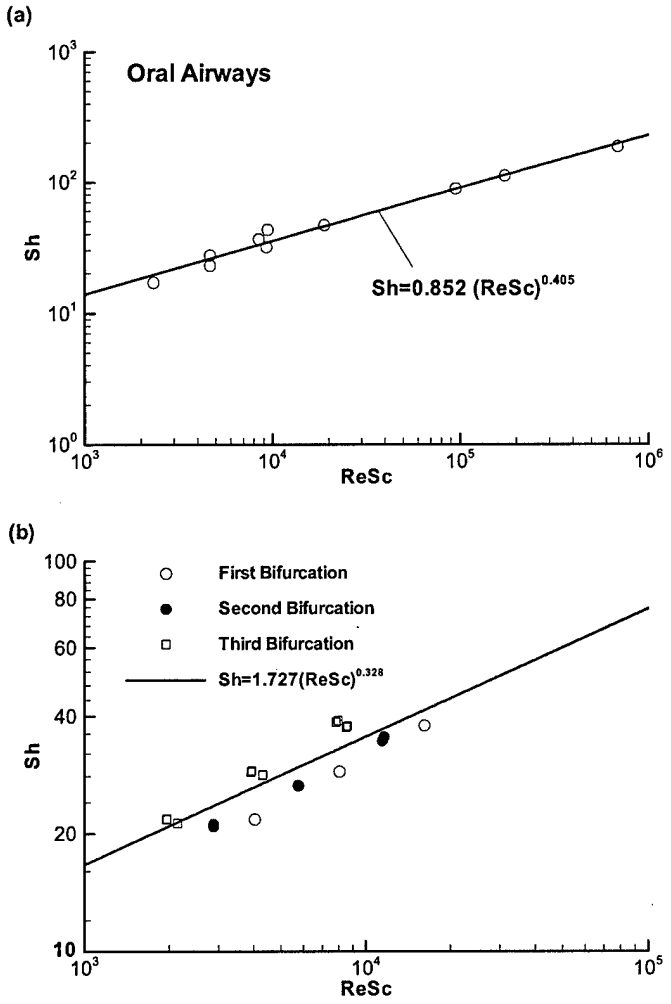

Fig. 12: Regional Sherwood number (Sh) versus the product of Re and Sc for: (a) human oral airways; and (b) human upper bronchial tree.

3.4.4 Impact of airway wall absorption parameter K

The absorption parameter K for different compounds of JP-8 fuel may vary from 10^{-3} to 10^{3}, resulting in large variations of the deposition fractions. Figure 13a shows the variation of deposition fraction in the oral and bifurcation airway models as a function of K. When K is less than one, the deposition is very low in the upper airways due to the low solubility of species in the mucus layer. The deposition fraction is greatly dependent on K for 1<K<1000. If K>1000, the deposition fraction is very close to that for the perfectly absorbing wall condition (i.e., Y_{wall}=0). The impact of K on the species mass transfer coefficients in the airways are depicted in Fig. 13b. Clearly, K almost has no effects on the mass transfer coefficients of species with the same diffusivities.

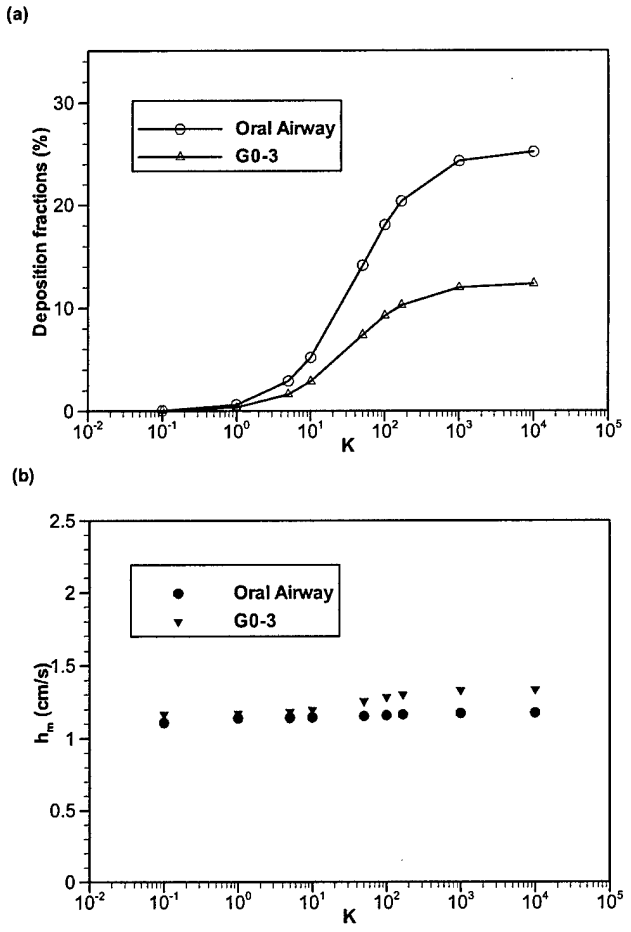

Fig. 13: The effects of airway wall absorption parameter K on: (a) deposition fraction and (b) mass transfer coefficients in the human upper airway model with Q_{in}=30 l/min and $\tilde{D}_a$ =0.05cm/s^2.

4. CONCLUSIONS

4.1 Fundamentals and New Discoveries

The first part of the three-year project focused on the fundamentals of "lung aerosol dynamics" and generated the following results:

(1) *Matching* Stokes and Reynolds numbers of cyclic inspiratory waveforms, i.e., the average between mean and peak values, was found to generate about the same particle deposition under cyclic flow condition as steady-state simulation results. Hence, with the corresponding matching Reynolds and Stokes numbers, the extrapolation of constant-flow deposition data to cyclic-flow situation at low Womersley numbers is possible (see Zhang et al., 2002a, b).

(2) The Low-Reynolds-number (LRN) k-ω model for internal flow was found to be appropriate for simulating all airflow regimes, i.e., laminar, transitional and turbulent, in the human upper airways (see Kleinstreuer & Zhang, 2003; Zhang & Kleinstreuer, 2003a; Zhang et al., 2002c).

(3) Depositions of both micro- and nano-size particles vary measurably in the human upper airways; however, the deposition distributions are much more uniform for nanoparticles. The maximum deposition enhancement factor, which is defined as the ratio of local to average deposition concentrations, ranges from about 40 to 2400 for microparticles and about 2 to 11 for nanoparticles with inspiratory flow rates in the range of $15 \leq Q_{in} \leq 60$ l/min. The nearly uniform distribution of deposited nanoparticles may imply greater toxicity effects of such particles when compared to microparticles made of the same material (see Zhang & Kleinstreuer, 2004; Zhang et al., 2005).

4.2 JP-8 Jet Fuel Droplets and Vapor

The transport and deposition of JP-8 jet fuel droplets and vapor in a human upper airway model were simulated and analyzed for different quasi-steady inhalation conditions. The experimentally validated CFPD results show the following:

(1) Thermal effects in the oral airways are considerable at low-level breathing (Q_{in}=15 l/min), where changing temperature distributions influence the velocity fields measurably, especially in the trachea. However, thermal effects tend to be minor for medium to high-level breathing (Q_{in}=30 to 60 l/min). Thermal effects in the bronchial airways are minor for all inhalation flow rates due to the warming-up of the air when moving through the oral airways.

(2) JP-8 fuel droplet evaporation greatly affects deposition concentrations in human airways. Droplet deposition fractions due to evaporation decrease with elevated ambient temperatures and lower inspiratory flow rates.

(3) Assuming idealized inlet velocity profiles and droplet distributions may greatly overpredict droplet deposition efficiencies for, say, $d_p \geq 3\mu m$, in the upper bronchial tree.

(4) Although the local vapor concentrations may be affected by non-isothermal flow, the total and segmental deposition fractions of (JP-8) fuel vapor in the upper airways are basically not influenced by variations in ambient temperature, i.e., $263K \leq T_{in} \leq 310K$, where the variation of deposition fractions is within 15%.

(5) The flow rate has a significant effect on fuel vapor deposition, i.e., the higher the flow rate the lower is the deposition fraction; for example, the deposition fraction in the present system, i.e., mouth to generation G3, changes from 30% to 60% when switching from high-level to low-level inhalation.

(6) The airway wall absorption of different JP-8 fuel components may greatly influence fuel vapor deposition

(7) As with micro-size droplets, deposition of vapor occurs to a greater extent around the carinal ridges when compared to the straight segments in the bronchial airways; however, vapor deposition distributions are much more uniform along the airway branches. Such a near-uniform distribution of deposited vapor also implies that more sites may interact with cell membranes, hence there is a higher probability of transport of toxic substances into tissue/blood.

4.3 Transitions

- U.S. EPA, Health Effects Research Laboratory (Dr. C. S. Kim)
  - **Result**: Computational aerosol inhalation studies of focal fuel droplet as well as ethanol and MTBE vapor depositions in a human upper airway models
  - **Application**: Validated toxic material deposition results are being used by the EPA for dosimetry-and-health-effect investigations, involving experimentalists, toxicologists, and pathway modelers. In summary, the AFOSR-sponsored technology can play a major role in analyzing cause-and-effect scenarios and ultimately justifying revised and new air pollution standards.

- Lovelace Respiratory Research Institute (LRRI), Inhalation Drug Delivery Center (Dr. Y.S. Cheng)
  - **Result**: Data exchange and supply of human cast models

- UNC-CH, Division of Pulmonary and Critical Care Medicine (Dr. J. Donohue)
  - **Result**: Supply of project findings to UNC-CH

- CIIT Centers for Health Research (Dr. Julie Kimbell)
  - **Result**: Information exchange

REFERENCES

AEA Technology (2001) *CFX-4.4: Solve*, Oxfordshire, UK: CFX International.

Balásházy, I., Hofmann, W. and Heistracher, T. (1999) "Computation of local enhancement factors for the quantification of particle deposition patterns in airway bifurcations". Journal of Aerosol Science 30: 185-203.

Balásházy, I., Hofmann, W. and Heistracher, T. (2003) "Local particle deposition patterns may play a key role in the development of lung cancer". J. Appl. Physiol., 94:1719-1725.

Bejan, A. (1995) *Convection Heat Transfer*, New York: John Wiley & Sons, Inc.

Broday, D.M. and Georgopoulos, P. G. (2001) "Growth and deposition of hygroscopic particulate matter in the human lungs". Aerosol Science and Technology 34: 144-159.

Cheng, K.H., Cheng, Y.S., Yeh, H.C. and Swift, D.L. (1997a) "An experimental method for measuring aerosol deposition efficiency in the human oral airway". Am. Ind. Hyg. Assoc. J. 58(3):207-213.

Cheng, K.H., Cheng, Y.S., Yeh, H.C. and Swift, D.L. (1997b) "Measurements of airway dimensions and calculation of mass transfer characteristics of the human oral passage". Journal of Biomechanical Engineering -Trans of the ASME 119:476-482.

Cheng, Y. S., Zhou, Y., and Chen, B. T. (1999) "Particle deposition in a cast of human oral airways". Aerosol Sci. Technol. 31:286-300.

Cohen, B.S., Sussman, R. G. and Lippmann, M. (1990) "Ultrafine particle deposition in a human tracheobronchial cast". Aerosol Sci. and Technol. 12:1082-1091.

Comer, J. K., Kleinstreuer, C. and Zhang, Z. (2001a) "Flow structures and particle deposition patterns in double bifurcation airway models. Part 1. air flow fields". Journal of Fluid Mechanics 435: 25-54.

Comer, J. K., Kleinstreuer, C. and Kim, C. S. (2001b) "Flow structures and particle deposition patterns in double bifurcation airway models. Part 2. aerosol transport and deposition". Journal of Fluid Mechanics 435: 55-80.

COT/NA (2003). *Toxicologic Assessment of Jet-Propulsion Fuel 8*, National Academies press.

Fan, B.J. Cheng, Y.S. and Yeh, H.C. (1996) "Gas collection efficiency and entrance flow effect of an annular diffusion denuder". Aerosol Sci. and Technol. 25(2):113-120.

Ferron, G.A., Kreyling, W. G. and Haider, B. (1988) "Inhalation of salt aerosol particles II. Growth and deposition in the human respiratory tract". J. Aerosol Sci. 19(5): 611-631.

Ferron, G. A., Oberdörster, G. and Henneberg, R. (1989) "Estimation of the deposition of aerosolized drugs in the human respiratory tract due to hygroscopic growth". J. Aerosol Med. 2: 271-284.

Finlay, W. H. (2001) *The Mechanics of Inhaled Pharmaceutical Aerosols: An Introduction*, London, UK: Academic Press.

Finlay, W. H., and Stapleton, K. W. (1995) "The effect on regional lung deposition of coupled heat and mass transfer between hygroscopic droplets and their surrounding phase". J. Aerosol Sci. 26(4): 655-670.

Gebheart, J., Anselm, A., Ferron, G., Heyder, J. and Stahlhofen, W. (1990) "Experimental data on the total deposition of hygroscopic particles in the human respiratory tract", in S. Masuda and K. Takahashi (eds) *Aerosols: Science, Industry, Health and Environment*, Oxford: Pergamon Press, pp.1299-1302.

Gustafson, J.B., Tell, J.G., Orem, D. (1997) *Selection of Representative TPH Fractions Based on Fate and Transport Consideration*, Amherst, MA: Amherst Scientific Publishers.

Hickey, A.J. and Martonen, T. B. (1991) "Behavior of hygroscopic pharmaceutical aerosols and the influence of hydrophobic additives". Pharm. Res. 10: 1-7.

Keyhani, K., Scherer, P. and Mozell, M.M. (1997) "A numerical model of nasal odorant transport for the analysis of human olfaction". J. Theor. Biol. 186: 279-301.

Kleinstreuer, C. (2003) *Two –Phase Flow: Theory & Applications*, New York: Taylor & Francis.

Kleinstreuer, C. and Zhang, Z. (2003) "Laminar-to-turbulent fluid-particle flows in a human airway model". Int. J. Multiphase Flow 29: 271-289.

LI, W., Xiong, J.Q., Cohen, B.S. (1998) "The deposition of unattached radon progeny in a tracheobronchial cast as measured with iodine vapor". Aerosol Sci. and Technol. 28: 502-510.

Morrow, P. E. (1986) "Factors determining hygroscopic aerosol deposition in airways". Physiol. Rev. 66: 330-376.

Runge, T., Teske, M. and Polymeropoulos, C.E. (1998) "Low-Temperature Vaporization of JP-4 and JP-8 Fuel Droplets". Atomiz. Sprays 8: 25-44.

Shi, H., Kleinstreuer, C., Zhang, Z. and Kim, C. S. (2004) "Nano-Particle Transport and Deposition in Bifurcating Tubes with Different Inlet Conditions". Physics of Fluids, 16: 2199-2213

Weibel, E. R. (1963) *Morphometry of the Human Lung*, New York: Academic Press.

Wilcox, D. C. (1993) *Turbulence Modeling for CFD,* LA Canada, CA: DCW Industries, Inc.

Zhang, Z. and Kleinstreuer, C. (2002) "Transient airflow structures and particle transport in a sequentially branching lung airway model". Physics of Fluids 14: 862-880.

Zhang, Z. and Kleinstreuer, C. (2003a) "Low Reynolds number turbulent flows in locally constricted conduits: a comparison study". AIAA Journal 41: 831-840.

Zhang, Z. and Kleinstreuer, C (2003b) "Species heat and mass transfer in a human upper airway model". International Journal of Heat and Mass Transfer, 46: 4755-4768.

Zhang, Z., and Kleinstreuer, C (2004) "Airflow Structures and Nano-Particle Deposition in a Human Upper Airway Model". Journal of Computational Physics 198: 178-210.

Zhang, Z., Kleinstreuer, C., Donohue, J. F. and Kim, C. S. (2005) "Comparison of micro- and nano-size particle depositions in a human upper airway model". J. Aerosol Sciences 36: 211-233.

Zhang, Z., Kleinstreuer, C. and Kim, C. S. (2002a) "Cyclic micron-size particle inhalation and deposition in a triple bifurcation lung airway model". J. Aerosol Sciences 33: 257-281.

Zhang, Z., Kleinstreuer, C. and Kim, C.S. (2002b) "Aerosol deposition efficiencies and upstream release positions for different inhalation modes in an upper bronchial airway model". Aerosol Science & Technology 36: 828-844.

Zhang, Z., Kleinstreuer, C., and Kim, C.S. (2002c) "Micro-particle transport and deposition in a human oral airway model". J. Aerosol Science 33: 1635-1652.

Zhang, Z., Kleinstreuer, C. and Kim, C.S. (2002d) "Gas-solid two-phase flow in a triple bifurcation lung airway model". Int. J. Multiphase Flow 28: 1021-1046.

Zhang, Z., Kleinstreuer, C., Kim, C. S. and Cheng, Y. S. (2004) "Vaporizing micro-droplet inhalation, transport and deposition in a human upper airway model". Aerosol Science and Technology 38: 36-49

Appendix A: List of Publications

(Air Force Grant, 08/15/01-08/14/04)

Journal Articles:

Zhang, Z., Kleinstreuer, C. and Kim, C.S., 2002, "Cyclic Micron-size Particle Inhalation and Deposition in a Triple Bifurcation Lung Airway Model", *J. Aerosol Science*, Vol. 33, pp. 257-281.

Zhang, Z., and Kleinstreuer, C, 2002, "Transient Airflow Structures and Particle Transport in a Sequentially Branching Lung Airway Model", *Physics of Fluids*, Vol.14, pp.862-880.

Zhang, Z., Kleinstreuer, C. and Kim, C.S., 2002, "Aerosol Deposition Efficiencies and Upstream Release Positions for Different Inhalation Modes in an Upper Bronchial Airway Model", *Aerosol Science & Technology*, Vol. 36, pp. 828-844.

Zhang, Z., Kleinstreuer, C. and Kim, C.S., 2002, "Gas-Solid Two-Phase Flow in a Triple Bifurcation Lung Airway Model", *Int. J. Multiphase Flow*, Vol. 28, pp. 1021-1046.

Zhang, Z., Kleinstreuer, C., and Kim, C.S., 2002, "Micro-Particle Transport and Deposition in a Human Oral Airway Model", *J. Aerosol Science*, Vol. 33, pp. 1635-1652.

Kleinstreuer, C., and Zhang, Z., 2003, "Laminar-to-Turbulent Fluid-Particle Flows in a Human Airway Model", *Int. J. Multiphase Flow*, Vol. 29, pp. 271-289.

Zhang, Z. and Kleinstreuer, C., 2003, "Low Reynolds Number Turbulent Flows in Locally Constricted Conduits: A Comparison Study", *AIAA Journal*, Vol. 41, 831-840.

Zhang, Z., and Kleinstreuer, C, 2003, "Species Heat and Mass Transfer in a Human Upper Airway Model", *International Journal of Heat and Mass Transfer*, Vol. 46, 4755-4768.

Zhang, Z., and Kleinstreuer, C, 2003, "Computational Thermodynamics Analysis of Vaporizing Fuel Droplets in the Human Upper Airways", *JSME International Journal*, Vol. 46, 563-571.

Zhang, Z., Kleinstreuer, C., Kim, C. S. and Cheng, Y. S., 2004, "Vaporizing Micro-Droplet Inhalation, Transport and Deposition in a Human Upper Airway Model", *Aerosol Science and Technology*, Vol.38, 36-49.

Zhang, Z., and Kleinstreuer, C, 2004, "Airflow Structures and Nano-Particle Deposition in a Human Upper Airway Model", *Journal of Computational Physics*, Vol. 198, 178-210.

Longest, P.W. and Kleinstreuer, C., 2004, "Interacting Effects of Uniform Flow, Plane Shear, and Near-Wall Proximity on the Heat and Mass Transfer of Respiratory Aerosols", International Journal of Heat and Mass Transfer, Vol. 47, 4745-4759.

Zhang, Z., Kleinstreuer, C, Donohue, J.F. and Kim, C. S., 2005, "Comparison of Micro- and Nano-Size Particle Depositions in a Human Upper Airway Model", *Journal of Aerosol Science*, Vol. 36(2), 211-233.

Longest, P.W. and Kleinstreuer, C., 2005, "Computational Models for Simulating Multicomponent Aerosol Evaporation in the Upper Respiratory Airways", *Aerosol Science and Technology*, in press.

Conferences Papers:

Kleinstreuer, C., Zhang, Z., and Kim, C.S., 2001, "Microscale Analysis and Simulation of the Air-Particle Dynamics in the Upper Respiratory System", *2001 Annual Meeting of the American Association for American Aerosol Research*, Portland, Oct. 15-19.

Zhang, Z., Kleinstreuer, C. and Kim, C.S., 2001, "Aerosol Transport and Deposition in a Triple Bifurcation Airway Model with Cyclic Inhalation and Exhalation", *2001 Annual Meeting of the American Association for American Aerosol Research*, Portland, Oct. 15-19.

Zhang, Z., Kleinstreuer, C. and Kim, C.S., 2001, "Transient Air Flow and Particle Transport in an Upper Tracheobronchial Airway Model", 2001 Annual Fall Meeting of the Biomedical Engineering Society, Durham, NC, USA, Oct. 4-7; *Annals of Biomedical Engineering*, Vol. 29, S139.

Kleinstreuer, C., Zhang, Z., and Kim, C.S., 2002, "Simulations and Analyses of Aerosol Deposition on Tumors in a Lung Airway Model", *21st Annual AAAR Conference*, Charlotte, NC, Oct. 7-11.

Zhang, Z., Kleinstreuer, C. and Kim, C.S., 2002, "Modeling of Air Flow and Particle Deposition in the Upper Human Airway", *21st Annual AAAR Conference*, Charlotte, NC, Oct. 7-11.

Zhang, Z. and Kleinstreuer, C., 2003, "Computational Thermodynamics of Aerosol Transport and Deposition in the Human Respiratory System", *Proceedings of 6th ASME/JSME Thermal Engineering Conference*, Hawaii, March 16-20.

Longest, P.W. and Kleinstreuer, C., 2003, "Multi-Scale Computational Analyses of JP-8 Jest-Fuel Aerosols in a Human Upper Respiratory Model", *2003 JP-8 Jest Fuel Exposure and Health Effects Symposium*, Tucson, AZ, May 14-16.

Zhang, Z., Shi, H., Kleinstreuer, C., and Kim, C. S., 2003, "Transport and Deposition of Nano-Size Particles in the Upper Human Respiratory Airways", *22nd Annual Conference of AAAR*, Anaheim, CA, Oct. 20-24.

Zhang, Z. and Kleinstreuer, C., 2004, "Computational Analysis of Two-Phase Air-Particle Flow in a Human Airway Model", *5th International Conference on Multiphase Flow, ICMF'04*, Yokohama, Japan, May 30–June 4.

Kleinstreuer, C., Longest, P. W., and Zhang, Z., 2004, "Theory of Biofluid Flow Dynamics and Selected Applications", Invited talk at *ASME Heat Transfer/Fluids Engineering Summer Conference*, July 11-15, Charlotte, North Carolina, USA.

Appendix B: Scientific Personnel Support

- **PI Dr. Clement Kleinstreuer,** Professor (20%, 3years)
- **Dr. Zhe Zhang,** Research Assistant Professor (60 ~ 100%, 3 years)
- **Dr. Worth Longest,** Post-doc (100%, 10 months)
- **Wei Shi,** Gradate student (RA) (50%, 2 years)
- **Zheng Li,** Gradate student (RA) (50%, 1/2 years)

Appendix C: List of Collaborators

- **Dr. C. S. Kim,** Senior Scientist, U.S. EPA, Human Studies Division, RTP, NC. Dr. Kim provides experimental data sets for lung airway models, reviews our manuscripts, and advises on toxic particle characteristics

- **Dr. Y. S. Cheng,** Director, Inhalation Drug Delivery Center, LRRI, Albuquerque, NM. Dr. Kim provides experimental data sets for lung airway models, reviews our manuscripts, and advises on toxic particle characteristics

- **Dr. J. Donohue,** Chief of Pulmonary Division, UNC-CH School of Medicine. Dr. Donohue advises us on aerosol characteristics, lung diseases, etc.